Isolating the hydrodynamic triggers of the dive response in eastern oyster larvae

JD Wheeler[1], KR Helfrich[2], EJ Anderson[3,4], LS Mullineaux[1]

Running Head: Hydrodynamic triggers of oyster dive

[1] Biology Department, Woods Hole Oceanographic Institution, Woods Hole, Massachusetts, 02543

[2] Physical Oceanography Department, Woods Hole Oceanographic Institution, Woods Hole, Massachusetts, 02543

[3] Department of Mechanical Engineering, Grove City College, Grove City, Pennsylvania, 16127

[4] Applied Ocean Physics and Engineering Department, Woods Hole Oceanographic Institution, , Woods Hole, Massachusetts, 02543

Acknowledgements

Thanks to Elaine Luo, Brenna McGann, Susan Mills, Andre Price, and Anthony Ritchie for assistance with larval acquisition, culture, experiments, and thanks to Anna Wargula for turbulence tank measurements. Thanks to Margaret Byron, Karen Chan, Joseph Fitzgerald, Mimi Koehl, and Evan Variano for helpful discussions throughout this project, and two anonymous reviewers for suggestions. We gratefully acknowledge the culturing expertise of the Aquaculture Research Corporation in Dennis, Massachusetts, who supplied the larval oysters used in this study. This work was supported by NSF grant OCE-0850419, NOAA Sea Grant NA14OAR4170074, grants from the WHOI Coastal Ocean Institute, discretionary WHOI funds, a WHOI Ocean Life Fellowship to LM, and a Grove City College Swezey Fellowship to EA.

Abstract

Understanding the behavior of larval invertebrates during planktonic and settlement phases remains an open and intriguing problem in larval ecology. Larvae modify their vertical swimming behavior in response to water column cues in order to feed, avoid predators, and search for settlement sites. The larval eastern oyster (*Crassostrea virginica*) can descend in the water column via active downward swimming, sinking, or "diving", which is a flick and retraction of the ciliated velum to propel a transient downward acceleration. Diving may play an important role in active settlement, since diving larvae move rapidly downward in the water column and may regulate their proximity to suitable settlement sites. Alternatively, it may function as a predator-avoidance escape mechanism. We examined potential hydrodynamic triggers to this behavior by observing larval oysters in a grid-stirred turbulence tank. Larval swimming was recorded for two turbulence intensities and flow properties around each larva were measured using particle image velocimetry. The statistics of flow properties likely to be sensed by larvae (fluid acceleration, deformation, vorticity, and angular acceleration) were compared between diving and non-diving larvae. Our analyses showed that diving larvae experienced high average flow accelerations in short time intervals (approximately 1-2 seconds) prior to dive onset, while accelerations experienced by non-diving larvae were significantly lower. Further, the probability that larvae dove increased with the fluid acceleration they experienced. These results indicate that oyster larvae actively respond to hydrodynamic signals in the local flow field, which has ecological implications for settlement and predator avoidance.

Introduction

Many marine invertebrates have a planktonic larval dispersal period before settling to the seafloor as adults. Our understanding of how larval behavior may influence dispersal and transport across a range of spatial scales is limited (Metaxas and Saunders 2009), and larval responses to a variety of physical, chemical, and biological cues remain ongoing areas of research. Larval swimming can be impacted by turbulent flow fields, especially in the turbulent bottom boundary layer as larvae move towards the substratum (e.g. Butman 1987, Butman et al. 1988). However, the impact of turbulent flow on the behavior of individual larvae is not well characterized due to technical challenges in simultaneously quantifying larval swimming and the motion of the surrounding flow field. Recent advances (Fuchs et al. 2013, Wheeler et al. 2013) are now making such studies feasible.

Small swimming organisms in a turbulent ocean experience a complex fluid environment, and may potentially respond to different components of ambient flow conditions, such as temporal velocity gradients (acceleration), spatial velocity gradients governing fluid deformation and rotation (strain rate and vorticity, respectively), and temporal vorticity gradients (angular acceleration). Rapid behavioral responses to local flow conditions are better studied for zooplankton than for larvae: threshold flow deformation has been observed to trigger escape responses in copepods (Kiørboe et al. 1999) as well as multiple protists (Jakobsen 2001). Acceleration, meanwhile, has not been observed to produce a similar response, though both acceleration and deformation are strong components of the suction flow fields produced by feeding predators (Kiørboe et al. 1999; Jakobsen 2001; Holzman and Wainwright 2009). In vortical flows, small organisms (ranging from bacteria to larvae) tilt and reorient, a response that has been attributed to a physical mechanism involving the balance of viscous and gravitational

77 torques acting on the organism (see for example Jonsson et al. 1991; Pedley and Kessler 1992;
78 Chan 2012). In this study, we focus on the larvae of the eastern oyster, *Crassostrea virginica*,
79 to increase our understanding of rapid behavioral responses of marine invertebrate larvae, and
80 bivalves particularly, to flow conditions that they might experience in the field.

81 We chose oyster larvae for this study because they exhibit intriguing swimming
82 behaviors in turbulent flows characteristic of coastal benthic habitats. They swim using a
83 ciliated velum and so control their own swimming direction in still water, likely sensing their
84 orientation and swimming direction with respect to gravity using a statocyst structure (Galtsoff
85 1964). A specific behavior of interest in oyster larvae is a response known as "dive-bombing" or
86 "diving" (Finelli and Wethey 2003; Wheeler et al., 2013). Herein, we consider diving as a
87 transient response occurring over timescales of approximately one second, where larvae abruptly
88 accelerate downward, achieving speeds up to 1 cm s^{-1}, or approximately 50 body lengths s^{-1},
89 which is distinct from the sustained slower downward swimming behavior defined as diving in
90 Fuchs et al. (2013). Diving, as we have defined it, has been observed in a moderately turbulent
91 channel flow (Finelli and Wethey, 2003), and in low turbulence induced by a grid-stirred tank
92 (Wheeler et al. 2013). The cue or cues triggering the onset of the dive response are not well
93 understood: some population-level estimates of larval swimming velocity in flow suggest that
94 downward swimming increases in high turbulence (Fuchs et al. 2013), while others suggest that
95 larvae persist in upward swimming in high turbulence, and further, that the dive response
96 disappears in highly turbulent flow (Wheeler et al. 2013). As larval swimming responses in
97 turbulence appear to be highly variable at the population level, we seek to identify specific
98 triggers experienced consistently by larvae immediately prior to dive onset. It is important to
99 identify these cues because through diving, a larva can rapidly displace itself downward through

100 the water column. This behavior may therefore impact larval supply to the benthos, as diving
101 may help larvae avoid predators and/or identify and approach suitable settlement sites.
102 Larvae settling into oyster reefs and other complex benthic structures experience a
103 complex fluid environment which may impact settlement patterns (e.g. Nowell and Jumars 1984;
104 Butman 1987; Koehl 2007). Current field research on oyster reefs suggests a link between oyster
105 larval settlement patterns and turbulent flow over regions of settlement. Whitman and
106 Reidenbach (2012) observed that turbulent drag and shear fields were considerably higher over
107 live oyster reefs than mud flats and restoration reefs made of broken oyster or whelk shells.
108 Larvae were observed to settle preferentially on oyster reefs, followed by whelk shell restoration
109 sites, then oyster shell restoration sites, and not at all on mud flats. Settlement patterns suggest
110 that flow fields generated by rough relief and low levels of turbulence in interstitial spaces may
111 abet larval recruitment. Because oyster larvae display a dive response in turbulent conditions,
112 we want to determine whether or not larvae dive in response to local hydromechanical cues in
113 the turbulent flow field, such as flow acceleration, deformation, vorticity, or angular
114 acceleration.
115 When transitioning out of the water column to the benthos, oyster larvae experience
116 turbulent flow fields that may induce rapid downward diving responses. In this study, we
117 actively quantify the diving response observed in two turbulence regimes, and determine which
118 (if any) local hydromechanical signals induce the response, as well as the response timescales.
119 Further, we use a Bayesian approach to calculate probabilities of larval diving conditioned on
120 specified local hydromechanical conditions (e.g. the probability of a larva diving, supposing it
121 has experienced a specified flow acceleration for a specified length of time). This relationship
122 may be useful for understanding the ecological implications of larval responses in specific field

conditions, and for the integration of behavior into larval models. We determine these diving triggers by identifying diving larvae and their local flow conditions in experimentally generated grid-stirred turbulence, then comparing the conditions experienced by diving and non-diving larvae as they move through the turbulent fluid environment.

Methods

Experimental organism and larval culturing

Crassostrea virginica, the eastern oyster, is a mollusc species native to the North Atlantic. Adults inhabit coastal shallow waters and broadcast spawn into the plankton, where larvae reside as free-swimming planktotrophs for 2-3 weeks (Kennedy 1996). Larvae entering the final planktonic stage, referred to as pediveligers, develop a foot and commonly a pronounced eyespot which are used in aquacultural practice to denote competency to settle (Thompson et al. 1996).

We obtained such competent larvae from the Aquaculture Research Corporation in Dennis, Massachusetts, United States of America, in three separate spawns in the summers of 2011, 2012, and 2013. All spawns were retained prior to experiments in identical culture conditions: 3 μm-filtered, aerated seawater at ambient field temperature (20-22^{o} C) and salinity (33 psu), in covered 16 L plastic buckets. Larvae were kept at low densities to minimize interactions (~3000 larvae L^{-1}) and fed a suspension of haptophyte *Isochrysis sp.* once per day (375 mL filtered seawater with ~9 x 10^{5} cells mL^{-1}.) Larvae were given a minimum period of 8 hours to acclimate post-transport from the aquaculture facility, and used for experiments within two days of competency onset. A representative sample of larvae from the 2013 spawn were measured and examined for eyespots prior to their use in experiments: average larval width (perpendicular to hinge) was ~277 μm, average height (parallel to hinge) was ~264 μm , and percentage of larvae with eyespots was >80%.

Experimental set-up

169

170 The turbulence tank used in the experiments (see Wheeler et al. 2013 for schematic)
171 consists of a ~180 L plexiglass tank (44.5 x 44.5 x 90 cm) with two horizontal grid structures set
172 equidistant from the centre of the tank, connected by vertical rods in each corner. The grid
173 structures are made from 1 cm x 1cm plexiglass bars spaced 5 cm apart. Both grids are connected
174 to a motor above the tank by a vertical rod, which drives a simultaneous vertical oscillation in the
175 grids. The oscillation amplitude is 5 cm and the oscillation frequency is specified by the user to
176 induce flow fields of different turbulence intensity.

177 In the analysis described in this study, the larvae were subjected to two turbulence levels,
178 hereafter referred to as "unforced" and "forced" regimes: the first regime has no flow induced in
179 the tank (i.e. the grid frequency is 0 Hz) and the second regime has low forcing conditions with a
180 grid frequency of 0.25 Hz. The forced regime has an estimated energy dissipation rate of 2×10^{-3}
181 $cm^2 s^{-3}$, and has Kolmogorov and integral length scales of 0.14 cm and 3.02 cm, respectively,
182 roughly comparable to calm field conditions in tidal channels and estuarine flows (Gross &
183 Nowell 1985). Note that although the grid was not operating in the unforced case, there was
184 weak turbulent flow in the tank due to residual motions and possibly convection. The original
185 experiments additionally subjected larvae to more highly turbulent flow conditions with
186 dissipation rates ranging from 0.017 $cm^2 s^{-3}$ in a moderate turbulence regime to 0.667 $cm^2 s^{-3}$ in
187 the most highly turbulent regime, and associated Kolmogorov and integral length scales ranging
188 from 0.08 to 0.03 cm and 3.64 to 3.59 cm, respectively. These regimes were not examined in our
189 present study because the larval diving behavior disappears in more highly turbulent flow (see
190 Wheeler at el. 2013).

191 A vertical cross-section in the centre of the tank was illuminated by a pulsed near-
192 infrared laser (Oxford Lasers, Firefly 300 W, 1000 Hz, 808 nm) in a plane approximately 1 mm
193 thick. A high-speed monochrome camera (Photron Fastcam SA3, 1024 x 1024 pixel resolution)
194 was trained perpendicularly to the laser sheet, recording a ~3 x 3 cm two-dimensional field of
195 view (FOV).
196 The tank was maintained in an environmental chamber of fixed temperature (20^{o} C) and
197 filled with surface seawater filtered to particle size < 1 μm. Larvae were gently introduced into
198 the tank using a beaker to densities of 0.5 – 0.62 larvae mL^{-1}. The tank was subsequently
199 seeded with a 2.5 mL suspension of neutrally buoyant polystyrene passive particles (3.0-3.4 μm
200 diameter, 1.05 g cm^{-3}density, 5% weight by volume, Spherotech, Lake Forest, Illinois, USA) to a
201 density of ~4.2 x 10^{4} particles mL^{-1} for flow quantification by particle image velocimetry (PIV).
202 Preliminary experiments showed no effects of these artificial particles on larval swimming in
203 still water, when compared to both swimming in control filtered seawater and seawater seeded
204 with natural *Isochrysis* algae (of roughly comparable size and concentration), leading us to
205 conclude that artificial particles could be used in turbulence experiments without affecting
206 behavior.
207 Larval behavior was recorded for 5-6 separate 45 second intervals at 60 fps (with the
208 number of intervals depending on the spawn and the turbulence level). These intervals were
209 separated in time by approximately 5 minutes each to transfer images from the camera to the
210 computer as TIFF files (e.g. Figure 1A). Experiments were conducted under identical conditions
211 over three separate two day periods in the summers of 2011, 2012, and 2013, corresponding to
212 three separate spawns. Larvae were subjected to multiple randomly ordered turbulence levels,
213 though only the two lowest turbulence regimes were examined in the present study. Turbulence

214 treatment order has no observed effect on larval swimming velocity (Wheeler et al. 2013), so
215 eliminating measurements from these higher turbulence levels should not affect our results.
216 Separate batches of larvae were also pooled for this analysis. Analyses of mean vertical
217 swimming velocities in higher turbulence regimes, and separated by larval batches, are presented
218 for the 2011 and 2012 data in Wheeler et al. (2013).
219
220 *Larval tracking and local flow subtraction*
221 The following methodology for isolating larval swimming velocity from advection in the
222 local flow field was presented in Wheeler et al. (2013) and is summarized here, with the added
223 refinement of interpolating local flow velocities to larval positions. First, larvae were identified
224 by the following method: all TIFF files were imported into LabVIEW 2010 (National
225 Instruments) and average background intensity was subtracted. Larval centroid positions (*x* and
226 *z* coordinates) were identified using a fixed threshold particle size and intensity and recorded
227 along with larval size, in the frame which they appeared.
228 Second, observed larval trajectories were computed using an in-house MATLAB script
229 which tracked identified larvae from frame to frame according to a subsequent-frame tolerance
230 distance radius set by the user. Larval trajectories were truncated by five frames at both the
231 beginning and end of the trajectories due to uncertainties in centroid estimates in cases where
232 larvae passed laterally into and out of the focal plane, which caused larvae to appear diffuse and
233 out of focus. Instantaneous observed larval velocities, denoted $\boldsymbol{u}_{\mathrm{obs}} = [u_{\mathrm{obs}}, w_{\mathrm{obs}}]$ for each
234 larva, were computed using a central difference scheme of larval centroid position in time, so
235 that the velocity is defined centered in time between the two images.

Third, fluid velocity fields in the FOV were quantified using PIV imaging software LaVision DaVis (v.7.2). All TIFF files were imported into the software and velocity fields were computed using correlations (default FFT with Whittaker reconstruction) of most likely passive particle positions from frame to frame, using 16x16 pixel interrogation windows (with 7-8 particles per window, not distinguishable by eye in Figures 1A-1B). This process yielded two 64 x 64 spatial grids of horizontal and vertical flow velocity for each time step, corresponding to a grid spacing of 0.039 – 0.046 cm (varied slightly by spawn).

Fourth, fluid velocities local to larvae were subtracted from observed larval velocities to obtain larval swimming velocities by the following method. The velocity fields estimated by PIV were imported and converted to MATLAB data files and velocity vectors in an annulus around each larva were used to estimate the fluid velocity at the larval position at each time step. The radius of the annulus changed dynamically for each larva: the inner radius was the sum of the maximum individual larval radius and the grid spacing of the PIV data (16 pixels), and the outer radius was four times greater than the inner radius (Figure 1B). The inner radius of the annulus masked the larval presence in the PIV data, which might otherwise contaminate the PIV analysis for fluid velocity. The velocity data in the annulus were fit to a two-dimensional, second-order Taylor series function by least-squares. The flow velocity $\boldsymbol{u} = [u, w]$ local to a larva was then obtained by evaluating the function at the larval centroid position. This interpolated fluid velocity was subtracted from the observed larval velocity at that time step to obtain the larval swimming velocity $\boldsymbol{u}_s = [u_s, w_s]$. For each larva,

$$\boldsymbol{u}_s = \boldsymbol{u}_{\text{obs}} - \boldsymbol{u}.$$

Identification of dive response

The dive response was initially observed by eye in experimental footage and in individual larval vertical swimming velocity time series, where it was characterized by a rapid drop to high downward swimming velocities, followed by a slow deceleration over the span of several seconds to near-zero vertical swimming velocity. We described a larva as diving if it performed downward accelerations of at least 3.0 cm s^{-2} (approximately 150 body lengths s^{-2}) for minimally 2 time steps (1/30 s) and achieved negative vertical swimming velocities of at least -0.4 cm s^{-1}. These thresholds in vertical swimming acceleration and velocity were used to separate diving larvae from non-diving larvae in the subsequent analysis (example difference between diving and non-diving larvae velocity time series, Figure 1D).

Hydromechanical parameters detectable by larvae

In this section, we propose a suite of hydromechanical cues in the turbulent flow that are likely to be detectable by larvae. Because larvae can be divided into divers and non-divers, relevant potential cues experienced by these two groups (Figure 1E) can then be compared for statistical differences. Following Kiørboe and Visser (1999), one may isolate the various aspects of a turbulent flow to which a larva might respond. Potentially relevant hydromechanical triggers are fluid acceleration, deformation (strain rate), rotation (vorticity), and angular acceleration. Given a flow velocity $\boldsymbol{u}$ local to a larva having swimming velocity $\boldsymbol{u_s}$, on any given time step, we can calculate the following acceleration, strain rate, vorticity, and angular acceleration fields.

Acceleration measures the rate of change in fluid velocity and could potentially be perceived by a larva through its statocyst structure: a calcareous statolith would be displaced into the wall of the statocyst cavity due to inertia in an accelerating flow (Chia et al., 1981; Fuchs et

al., 2013). To characterize the temporal changes in flow velocity near an individual larva, we use the magnitude of the two-dimensional acceleration of the fluid flow following the larval position (Maxey and Riely 1983) (see the Web Appendix for a derivation):

$$|\boldsymbol{a}| = \left|\frac{\partial \boldsymbol{u}}{\partial t} + (\boldsymbol{u} + \boldsymbol{u_s}) \cdot \nabla \boldsymbol{u}\right|.$$

We use acceleration magnitude, with magnitude denoted by $|\cdot|$, as a hydromechanical metric in order to incorporate both dimensions of the acceleration vector. This acceleration metric excludes the acceleration that a larva experiences due to its own swimming motion, accounting only for the acceleration the larva experiences due to the local flow field. Larval swimming velocity $\boldsymbol{u_s}$ is present in $|\boldsymbol{a}|$ because both larval swimming and flow velocity contribute to larval position, hence the inclusion of both in the advection term. If larvae perceive acceleration using a statocyst, they would feel the total acceleration from both the flow and their own swimming (see Web Appendix). However, we focus on the externally-imposed fluid acceleration because it is independent of all larval behavior: this simplifies the interpretation of our results, as we do not conflate the larval responses to internally-imposed and externally-imposed motion.

In practice, the flow acceleration above is calculated by interpolating flow velocity to the larval position at each time step, then using a central difference scheme to compute the temporal derivative along the larval path. While the acceleration magnitude used in this analysis uses only the two known dimensions (x, z) available from our PIV set-up, the unknown y-acceleration component will be similar to that of x, due to tank and forcing symmetries. We estimated a three-dimensional acceleration magnitude by doubling the x-acceleration component

303 and found that the two and three dimensional fluid acceleration estimates yield similar statistical
304 results, so we report only the two-dimensional results in the subsequent sections.

305 The velocity gradients in a fluid flow lead to shear stresses on the surface of any object or
306 fluid parcel in that flow. The net effect of these shear stresses can be to strain (i.e. deform) and
307 rotate the object or fluid parcel. The strain rate (quantified using the rate of strain tensor)
308 determines how a fluid parcel is stretched or sheared in different spatial dimensions, and could
309 potentially be detected by a larva at sufficiently high signal strength by a deformation of cilia
310 along the velum. The rotation rate (quantified using the vorticity) is likely detectable through a
311 larva's statocyst structure (Chia et al. 1981), as the statolith is displaced and rolls steadily along
312 the statocyst cavity wall, imposing a centrifugal force.

313 Strain rate is quantified in a three dimensional flow by the symmetric strain rate tensor
314 e_{ij}, elements of which describe the deformation of the flow along two axes. Because we have
315 only two dimensions of velocity data, the full strain rate tensor cannot be computed, and we are
316 restricted to the examination of three of the elements of the tensor: the shear strain rate e_{xz} and
317 the normal strain rates e_{xx} and e_{zz}. We use the two-dimensional shear strain rate magnitude at
318 the larval position:

319

$$|e_{xz}| = \left|\frac{1}{2}\left(\frac{\partial u}{\partial z} + \frac{\partial w}{\partial x}\right)\right|.$$

320

321 This metric represents the shearing, or deformation, of a fluid parcel in the focal plane, and is
322 calculated using flow velocities local to the larval position. We use the magnitude of the shear
323 strain rate because the sign of this term simply governs the direction in which the shear
324 deformation occurs, and we do not expect larvae to recognize or respond to this directionality.

Normal strain rates are

$$e_{xx} = \frac{\partial u}{\partial x}$$

and

$$e_{zz} = \frac{\partial w}{\partial z},$$

where these quantities measure how fluid is stretched in the x and z dimensions, respectively, calculated local to the larval position at each time step. Unlike the shear strain rate, the signs of the normal strain rates are retained; positive normal strain rates indicate divergence in the specified spatial dimension, while negative normal strain rates indicate convergence in the specified spatial dimension, and these are physically distinct phenomena. For all strain rates, the spatial derivatives are calculated at the fluid velocity points in the annulus around each larva and then interpolated to the larval position using the method described for the velocity field in the local flow subtraction section.

Vorticity measures the rotation of a fluid parcel, and is likely detectable through a larva's statocyst structure, as described above. Vorticity is a three dimensional vector for a three dimensional flow, with each element describing the rotation of the fluid normal to a plane described by the other two dimensions. Because we have only two dimensions of velocity data, we are restricted to using the vorticity element normal to the focal plane as our vorticity metric:

$$|\omega_y| = \left|\frac{\partial w}{\partial x} - \frac{\partial u}{\partial z}\right|.$$

344 The vorticity is calculated local to larval position at each time step, with spatial derivatives
345 calculated as described above for the strain rate metrics. Similarly to shear strain rate, we define
346 our vorticity metric by the magnitude of the vorticity element: the sign of vorticity denotes the
347 direction of rotation of the local fluid (clockwise versus anti-clockwise), which we do not expect
348 the larvae to distinguish. In a simple parallel shear flow, vorticity is equal to the velocity
349 gradient in a single direction, and we use vorticity in this study because it generalizes the shear
350 metric commonly reported in simpler flows (Kiørboe and Visser 1999). Similar to the
351 acceleration term defined above, this vorticity term accounts only for the fluid rotation around
352 the larva and not the larva's own rotation term. The larval rotation term is not considered in this
353 analysis; as above, the rationale is to separate external forcing imposed by the fluid from the
354 internal forcing of the larva's own swimming motion.
355 Angular acceleration measures the rate of rotation of a fluid parcel, and may be
356 detectable in the larval statocyst structure through the onset of statolith motion along the
357 statocyst wall. To characterize the temporal changes in flow vorticity near an individual larva,
358 we compute the magnitude of the angular acceleration of the fluid flow following the larval
359 position:
360

$$|\alpha| = \left|\frac{\partial \omega_y}{\partial t} + (\boldsymbol{u} + \boldsymbol{u_s}) \cdot \nabla\, \omega_y\right|.$$

361
362 In practice, the angular acceleration is calculated by interpolating flow vorticity to the larval
363 position at each time step, then using a central difference scheme to compute the temporal
364 derivative along the larval path. To avoid confusion, in the following analysis and discussion,
365 *acceleration* always refers to $\boldsymbol{a}$, the rate of change of fluid velocity following larval paths, while

366 *angular acceleration* specifically will be used to refer to α, the rate of change of fluid vorticity
367 following larval paths.
368
369 *Statistical analysis*
370 In this study, one of our objectives was to determine differences in hydromechanical
371 parameters (flow acceleration, normal and shear strain rates, vorticity, and angular acceleration)
372 experienced by diving larvae and non-diving larvae. To determine this, we calculated mean
373 hydromechanical parameters experienced by all diving larvae in a set temporal interval
374 immediately prior to dive onset, and mean hydromechanical parameters in the same temporal
375 interval (randomly selected in the individual larval trajectory) for non-diving larvae. We used
376 means instead of maxima, as using mean values in short time intervals allowed us to capture
377 peak hydromechanical parameter values while filtering out PIV noise that distorts the maxima.
378 A randomly subsampled group of non-diving larvae were then selected to compare to the diving
379 larvae, so that the sample size in both groups would be identical. Two conditional probability
380 distributions were then constructed for comparative purposes: $P(T|\text{ larva dives})$ and
381 $P(T|\text{ larva does not dive})$ for each mean hydromechanical parameter T.
382 The distributions of mean hydromechanical parameters experienced by diving larvae and
383 non-diving larvae were then compared statistically using the following methods. If T was
384 strictly non-negative (i.e. all magnitude terms) we used a non-parametric 2-sided Wilcoxon rank
385 sum test to compare the medians of the diving versus non-diving distributions. If the
386 distributions were drawn from both positive and negative values, we used a modified 2-tailed *t*-
387 test (Welch's approximate *t*-test statistic and Satterthwaite's approximation for the degrees of
388 freedom) to compare the means of the distributions instead.

If a parameter was found to differ significantly between diving and non-diving larvae, both distributions were compared to the background distribution of the hydromechanical parameter, $P(T)$, which was determined by computing T through four fixed spatial points in the FOV over the three experiments (over comparable spatial and temporal scales to which T was computed for the larvae). The comparisons of diving, non-diving, and background T distributions were carried out using a non-parametric Kruskal-Wallis test. A multiple comparison test was subsequently carried out to identify whether hydromechanical parameters experienced by diving and/or non-diving larvae differed significantly from the average parameter values in the background flow. All statistical tests were carried out using MATLAB.

For any hydromechanical parameter which differed significantly between diving and non-diving larvae, the conditional probability of diving given a specified mean parameter value was calculated using Bayes theorem:

$$P(\text{larva dives} \mid T) = \frac{P(\text{larva dives}) \cdot P(T \mid \text{larva dives})}{P(T)}.$$

The probability of larval diving, $P(\text{larva dives})$, is the number of diving larval trajectories divided by the total number of trajectories observed, while $P(T \mid \text{larva dives})$ and $P(T)$ are described above. The conditional probability of larval diving given a mean hydromechanical parameter value, $P(\text{larva dives} \mid T)$, is an ecologically relevant function as it predicts larval behavior in response to specific environmental conditions.

A 95% confidence interval for this conditional probability was computed by summing in quadrature the independent confidence intervals from each term in the equation. Confidence intervals for $P(T \mid \text{larva dives})$ and $P(T)$ were estimated by bootstrapping the distributions and directly computing the confidence interval for each value of T. The confidence interval for the

411 scalar $P(\text{larva dives})$ was computed using the Clopper-Pearson method for binomial confidence
412 intervals as the diving probability is a probability of success in a binomial trial (i.e. diving vs.
413 non-diving).
414
415
416
417
418
419
420
421
422
423
424
425
426
427
428
429
430
431
432
433

Results

Identification of dive response

Using our quantitative definition of diving, we found that 82 larvae (of 874 total larvae) dove at least once during their observed trajectory in the unforced regime, and 57 larvae (of 1019 total larvae) dove at least once in the forced regime. We overlaid the diving trajectories aligned by dive onset time in the unforced regime (Figure 2) to identify similarities in diving trajectories, and found similar timescales in the downward acceleration for all larvae, on the order of 0.1 s. Larvae reached peak downward velocities ranging from -0.5 to -0.7 cm s^{-1} and decelerated to zero velocity in approximately one second. Prior to dive onset, larvae engaged in a range of vertical velocities, centered near zero, but both upward and downward swimming were observed, suggesting that larvae had no fixed pre-dive behavior. As larvae decelerated from the dive and resumed a more constant vertical velocity, they exhibited a similar range of vertical velocities, indicating that larvae also had no fixed post-dive behavior. Vertical displacement from a single dive was of order 10^{-1} cm, or approximately 4 body lengths, and comparable to the Kolmogorov scale, the length scale of the smallest eddies in the forced regime.

Hydromechanical parameters triggering the dive response

A range of temporal intervals prior to the dive onset was investigated, from 0.33s to 3s, in intervals of 0.33s (see Web Appendix) to identify potential reaction timescales for diving larvae. A hydromechanical parameter was considered to be a consistent trigger to the dive response only if 1) it differed significantly between diving and non-diving larvae in the specified

456 temporal interval, and 2) this significant response held in both flow regimes, unforced and
457 forced, for identical temporal intervals.

458 Diving larvae consistently experienced significantly higher mean acceleration than non-
459 diving larvae. In the unforced regime, mean accelerations were significantly higher for diving
460 larvae in the 1, 1.33, 1.66, and 2s time intervals and intermittently significant for longer time
461 intervals (Table 1,Figure 3A). In the forced regime, mean accelerations were significantly higher
462 for diving larvae in all time intervals from 1.33s to 3s prior to the dive onset (Table 1, Figure
463 3A). The intersection of these temporal intervals is 1.33 – 2.33s, representing the consistent
464 response range in which diving larvae experienced significantly higher acceleration than non-
465 diving larvae. For subsequent analyses presented in the main text, we used a central point of
466 this interval, 1.66s prior to dive onset, as the averaging window and denote the mean acceleration
467 experienced by a larva in this interval as $|\boldsymbol{a}|_{1.66}$.

468 No other hydromechanical parameter differed significantly prior to dive onset between
469 diving and non-diving larvae (Figures 3B-3F, Web Appendix Tables A1-A2) in contrast to
470 acceleration (Figure 3A, Table 1). That is, none of shear deformation, normal deformation
471 (horizontal or vertical), vorticity, or angular acceleration induced a diving response in larvae in
472 any temporal window examined.

473 Flow accelerations experienced by diving and non-diving larvae in the 1.66s interval
474 were then compared to background acceleration fields (Figure 4). These three distributions of
475 flow acceleration, $P(|\boldsymbol{a}|_{1.66}|\text{ larva dives})$, $P(|\boldsymbol{a}|_{1.66}|\text{ larva does not dive})$, and $P(|\boldsymbol{a}|_{1.66})$, were
476 significantly different in the unforced regime (Table 2). A post-hoc multiple comparison test of
477 these distributions demonstrated that diving larvae experienced significantly higher average flow
478 accelerations than both non-diving larvae and the average background acceleration. Non-diving

479 larvae experienced flow accelerations that were indistinguishable from the background
480 acceleration. In the forced regime, a similar pattern was observed: diving larvae experienced
481 higher accelerations than did non-diving larvae, as well as higher accelerations than those
482 occurring in the background flow. However, the result in this regime was non-significant (Table
483 2), likely due to the smaller sample size of dives and lower power of the multi-way comparison.
484 These distributions were then used to compute $P(\text{larva dives} \mid |\boldsymbol{a}|_{1.66})$, the conditional
485 probability that larvae dove for a given acceleration averaged over the 1.66s pre-dive window in
486 the unforced regime (Figure 5). The positive relationship between this probability and the
487 acceleration demonstrates that diving became a more probable response as mean fluid
488 acceleration experienced by larvae increased. The bounds on the 95% confidence intervals
489 increased for high acceleration values due to the rarity of high acceleration events, which likely
490 also accounted for overestimates of the conditional diving probability (i.e. greater than 1) for
491 high accelerations. The computation is omitted for the forced regime as the large decrease in
492 number of dives observed renders estimates much more uncertain.
493
494
495
496
497
498
499
500
501

Discussion

Comparisons of flow fields experienced by diving and non-diving larvae strongly support a conclusion that flow acceleration triggers the dive response in oyster larvae. Diving larvae experienced significantly higher mean fluid accelerations than did non-diving larvae during a short period leading up to the dive onset in both turbulence regimes. The other candidate hydromechanical parameters did not differ significantly between diving and non-diving larvae: none of mean normal strain rates, shear strain rate, vorticity, or angular acceleration triggered the dive response. An examination of diving in the central 1.66s response window demonstrated that not only did diving larvae experience higher accelerations than non-diving larvae, but that these accelerations were anomalously high compared to the background (significantly so in the unforced regime). The correspondence between probability of diving and increasing fluid acceleration further reinforces the interpretation that diving is triggered by acceleration. Further, the time interval over which the threshold mean acceleration was experienced was important for triggering the dive response. When acceleration was averaged over temporal windows shorter than 1.33s, higher acceleration did not appear to induce diving preferentially. This analysis suggests that the reaction timescale of the larvae to the fluid acceleration field they experience was at least 1.33s. A lack of pattern in timescales longer than 2s suggests that the larvae are responding to an acceleration event, roughly 1.5 s before the dive, rather than to mean acceleration over a longer interval.

The observation that a mean acceleration of 0.035 cm s^{-2} triggered a dive in the unforced case, but not in forced case, indicates that the required threshold acceleration changes with the turbulence level. In the low-forcing regime, an average acceleration of 0.06 cm s^{-1} triggered a

525 dive, while non-diving larvae experienced mean accelerations of 0.04 cm s^{-2}. This result suggests
526 that larvae become conditioned to the flow regime in which they find themselves, and the dive
527 response is triggered by anomalously high accelerations compared to the background
528 acceleration. This interpretation is supported by the finding that the accelerations experienced by
529 diving larvae were significantly higher than both non-diving larvae and the background field. In
530 a previous study (Wheeler et al. 2013), the dive response was found to disappear entirely in
531 highly turbulent flow conditions (having energy dissipation rates greater than 10^{-1} cm^2 s^{-3}).
532 While our experimental results do not provide a complete explanation for this disappearance, we
533 offer several possibilities. First, larvae may simply stop reacting to an acceleration trigger
534 above a certain threshold which occurs in the higher turbulence regimes. Second, recall that
535 larvae respond to anomalously high accelerations within a turbulence level, and this threshold
536 increases with turbulence intensity, at least in unforced and low forcing conditions. The
537 frequency with which larvae encounter sufficiently high acceleration anomalies in more
538 turbulent regimes may be lower, which would explain the lack of diving in these regimes.
539 However, we cannot quantify the diving threshold accelerations for these higher flow regimes
540 (beyond supposing the thresholds are greater than that observed in our low flow forced regime),
541 and as such, this explanation for the lack of diving in high turbulence remains speculative.
542 Alternatively, it is possible that the experimental set-up precluded detection of dives because
543 larvae are advected quickly in more highly turbulent flow. It is possible that it becomes more
544 difficult to observe the diving response because larvae remain in the FOV for shorter time
545 periods (though more larvae are observed in higher turbulence regimes).
546 The dive response for all observed larvae was highly uniform in terms of acceleration and
547 deceleration timescales (Figure 2), and the response is predictable based on fluid acceleration

548 through the conditional probability $P(\text{larva dives} \mid |\boldsymbol{a}|)$. These characteristics make the dive
549 response well suited for inclusion into individual based models of larval behavior in complex
550 flow fields (see for instance Koehl et al. 2007). Such models would be very useful for testing
551 whether diving affects settlement success in simulated turbulent flow fields over rough bottom
552 topography. The strong uniformity of the dive further suggests that the response, once
553 instigated, is regulated by biomechanical constraints, as all larvae emerge from the dive and
554 resume swimming on comparable timescales. In this way, the diving response triggered by
555 acceleration may differ from the sinking response to waterborne chemical cues observed in the
556 larval sea slug *Phestilla sibogae* (Hadfield and Koehl 2004). These larvae retract velar lobes
557 instantly in response to coral-conditioned seawater, and continue to sink unless the cue is absent
558 on timescales of one second or longer. Our larvae, conversely, cease to dive after approximately
559 1 second regardless of local flow conditions. While the larvae are capable of diving multiple
560 times in succession, their behavior appears distinct from the sustained sinking observed in *P.*
561 *sibogae* larvae.

562 The effects of local environmental conditions on the behavior of mollusc larvae have
563 been previously studied in a few species with varying results. Two bivalve larvae (*Crassostrea*
564 *gigas* and *Mytilus edulis*) exposed to horizontal suction flow demonstrated no discernible
565 swimming response as they approached a suction tube (Troost et al. 2008), a flow that would
566 have a strong acceleration signal. However, the flow fields experienced by these larvae were
567 quantified in a separate experiment from the larval observations. This technique can make it
568 difficult to isolate larval behavior (Wheeler et al. 2013), as small scale temporal and spatial
569 variations in the flow field that larvae might experience are not captured. *P. sibogae* retract their
570 velar lobes in response to mechanical stimulus (Hadfield and Koehl 2004), and potentially to

local hydrodynamic conditions (M. Koehl, *personal communication*), as well as the potentially distinct response to chemical cues, as discussed above. The similarity of the response (retraction of ciliated swimming organ into a shell) in different mollusc groups suggests that larval diving in response to acceleration may be common to multiple species.

A dive response when larvae are experiencing anomalously high accelerations could potentially be a beneficial strategy if they need to settle onto rough bottom surfaces, or to avoid predator feeding currents. We consider both possibilities, beginning with the ecological implications of diving as a settlement response. PIV measurements over rough topography in an oscillating flow tank have demonstrated that the highest accelerations occur up to 5 cm from the bottom, and decay rapidly farther above (R. Pepper, J. Jaffe, E. Variano, and M. Koehl, *personal communication*). Further, simulated larvae in the PIV-measured flow experience peak accelerations of short duration that are much higher in magnitude than the mean values, much like the anomalously high accelerations experienced by the diving larvae in our study. The threshold accelerations experienced by larvae in our unforced and forced regimes are small compared to the fluid accelerations near the bottom reported by Pepper et al., but may help larvae navigate downward through the water column at heights above 5 cm from the bottom. The dive response disappears in more highly turbulent flow regimes that more closely mimic the energetics of flow immediately above preferred settlement sites (e.g. Whitman and Reidenbach 2012), which offers further evidence the dive response is likely to be employed by larvae higher in the water column.

Larvae could alternatively experience flow acceleration due to suction feeding flows from predators in the plankton (Kiørboe et al. 1999; Jakobsen 2001; Holzman and Wainwright 2009) or even from the feeding currents of adult oysters on reefs (Troost et al. 2008). In this

way, the dive could act as an escape response analogous to the jumping behavior of copepods (e.g. Waggett and Buskey 2007; Lee et al. 2010) or the rapid downward swimming of insect larvae and pupae (e.g. Aswathi et al. 2012) observed in the presence of predators. Larval dive responses to flow acceleration in the water column could thus increase larval supply to the seafloor, by either increasing the rate of downward flux, or decreasing the proportion lost to predators.

References

Awasthi A.K., C.-H. Wu, and J.-S. Hwang. 2012. Diving as an anti-predator behavior in mosquito pupae. Zool. Stud. **51**: 1225-1234.

Butman C. 1987. Larval settlement of soft-sediment invertebrates: The spatial scales of pattern explained by active habitat selection and the emerging role of hydrodynamical processes. Oceanogr. Mar. Biol. **25**: 113–165.

Butman C, J. Grassle, and C. Webb. 1988. Substrate choices made by marine larvae settling in still water and in a flume flow. Nature **333**: 771–773.

Chan, K. 2012. Biomechanics of larval morphology affect swimming: Insights from the sand dollars *Dendraster excentricus*. Integr. Comp. Biol. **52:** 458--469.

Chia F., R. Koss, and L. Bickell. 1981. Fine structural study of the statocysts in the veliger larva of the nudibranch, *Rostanga pulchra*. Cell Tissue Res. **214:** 67--80.

Finelli C., and D. Wethey. 2003. Behavior of oyster (*Crassostrea virginica*) larvae in flume boundary layer flows. Mar. Biol. **143**: 703–711.

Fuchs H.L., E.J. Hunter, E.L. Schmitt, and R.A Guazzo. 2013. Active downward propulsion by oyster larvae in turbulence. J. Exp. Biol., **216**: 1458-1469.

637 Galtsoff P.S. 1964. The American Oyster *Crassostrea virginica* (Gmelin). U.S. Fish Wildl.
638 Serv. Fish. Bull. **64**: 1-480.
639
640 Gross T., and A. Nowell. 1985. Spectral scaling in a tidal boundary layer. J Phys. Oceanogr. **15**:
641 496–508.
642
643 Hadfield M., and M. Koehl. 2004. Rapid behavioral responses of an invertebrate larva to
644 dissolved settlement cue. Biol. Bull. **207**: 28--43.
645
646 Holzman R., and P. Wainwright. 2009. How to surprise a copepod: Strike kinematics reduce
647 hydrodynamic disturbance and increase stealth of suction-feeding fish. Limnol. Oceanogr. **54**:
648 2201--2212.
649
650 Jakobsen, H. 2001. Escape response of planktonic protists to fluid mechanical signals. Mar.
651 Ecol. Prog. Ser. **214**: 67--78.
652
653 Jonsson P., C. Andre, M. Lindegarth. 1991. Swimming behavior of marine bivalve larvae in a
654 flume boundary-layer flow: Evidence for near-bottom confinement. Mar. Ecol. Prog. Ser. **79**:
655 67--76.
656
657 Kennedy V.S. 1996. Biology of larvae and spat. Pp. 371--421. *In* V.S. Kennedy, R.I.E.
658 Newell, and A.F. Eble [eds.], The Eastern Oyster (*Crassostrea Virginica*). Maryland Sea Grant.
659

660 Kiørboe T., and A. Visser. 1999. Predator and prey perception in copepods due to
661 hydromechanical signals. Mar. Ecol. Prog. Ser. **179**: 81--95.
662
663 Kiørboe T., E. Saiz, and A. Visser. 1999. Hydrodynamic signal perception in the copepod
664 *Acartia tonsa*. Mar. Ecol. Prog. Ser. **179**: 97--111.
665
666 Koehl M. 2007. Mini review: Hydrodynamics of larval settlement into fouling communities.
667 Biofouling **23**: 357—368.
668
669 Koehl M., J. Strother, M. Reidenbach, J. Koseff, M. Hadfield. 2007. Individual-based model of
670 larval transport to coral reefs in turbulent, wave-driven flow: Behavioral responses to dissolved
671 settlement inducer. Mar. Ecol. Prog. Ser. **335**: 1--18.
672
673 Lee C.-H., H.-U. Dahms, S.-H. Cheng, S. Souissi, F.G. Schmitt, R. Kumar, and J.-S. Hwang.
674 2010. Predation of *Psudodiaptomus annandalei* (Copepoda: Calanoida) by the grouper fish fry
675 *Epinephelus coioides* under different hydrodynamic conditions. J. Exp. Mar. Biol. Ecol. **393**:
676 17-22.
677
678 Metaxas A., and M. Saunders. 2009. Quantifying the bio- components in biophysical models of
679 larval transport in marine benthic invertebrates: Advances and pitfalls. Biol. Bull. **216**: 257--
680 272.
681

682 Maxey M.R., and J.J. Riley. 1983. Equation of motion for a small rigid sphere in a non-uniform
683 flow. Phys. Fluids **26**: 883-889.
684
685 Nowell A., and P. Jumars. 1984. Flow environments of aquatic benthos. Annu. Rev. Ecol. Sys.
686 303-328.
687
688 Pedley T., and J.Kessler. 1992. Hydrodynamic phenomena in suspensions of swimming
689 microorganisms. Annu. Rev. Fluid Mech. **24**: 313--358.
690
691 Thompson R., R.I.E. Newell, V.S. Kennedy, R. Mann. 1996. Reproductive processes and early
692 Development. Pp. 335—370. *In* V.S. Kennedy, R.I.E. Newell, and A.F. Eble [eds.], The
693 Eastern Oyster (*Crassostrea Virginica*). Maryland Sea Grant.
694
695 Troost K., R. Veldhuizen, E. Stamhuis, and W. Wolff. 2008. Can bivalve veligers escape
696 feeding currents of adult bivalves? J. Exp. Mar. Biol. Ecol. **358**: 185--196.
697
698 Waggett R.J., and E.J. Buskey. 2007. Calanoid copepod escape behavior in response to a visual
699 predator. Mar. Biol. **150**: 599-607.
700
701 Wheeler J.D., K.R. Helfrich, E.J. Anderson, B. McGann, P. Staats, A.E. Wargula, K. Wilt, and
702 L.S. Mullineaux . 2013. Upward swimming of competent oyster larvae (*Crassostrea virginica*)
703 persists in highly turbulent flow as detected by PIV flow subtraction. Mar. Ecol. Prog. Ser. **488**:
704 171 −185.

Whitman E.R., and M.A. Reidenbach. 2012. Benthic flow environments affect recruitment of *Crassostrea virginica* larvae to an intertidal oyster reef. Mar. Ecol. Prog. Ser. **463**: 177-191.

Tables

Table 1: Wilcoxon rank sum test comparing medians of mean acceleration distributions experienced by diving versus non-diving larvae, where means are computed in the stated window prior to dive onset. The null hypothesis states that medians $M_{\mathrm{d}} = M_{\mathrm{nd}}$ while the alternate hypothesis states that they differ. Significance level is $\alpha = 0.05$. The medians of mean acceleration distributions are significantly higher for diving larvae than non-diving larvae in both flow regimes, given at least a 1.33s window over which local acceleration is averaged.

Time interval prior to dive onset (s)	Turbulence regime	Rank sum	z	p-value
0.33	Unforced regime $\varepsilon \to 0$ cm^2 s^{-3}	6314	1.84	0.06
0.66		6270	1.67	0.09
1.00		6490	2.48	**0.01**
1.33		6735	3.39	**<0.001**
1.66		6697	3.25	**0.001**
2.00		6406	2.17	**0.02**
2.33		6148	1.22	0.21
2.66		6626	2.99	**0.002**
3.00		6318	1.88	0.06
0.33	Forced regime $\varepsilon = 10^{-3}$ cm^2 s^{-3}	3095	1.63	0.10
0.66		3076	1.51	0.13
1.00		3015	1.13	0.25
1.33		3166	2.08	**0.03**
1.66		3164	2.07	**0.03**
2.00		3325	3.08	**0.002**
2.33		3232	2.50	**0.01**
2.66		3144	1.94	**0.05**
3.00		3244	2.57	**0.009**

735 Table 2: Kruskal-Wallis test comparing median average accelerations experienced by the
736 following three groups: diving larvae in a 1.66 s window prior to dive onset, non-diving larvae in
737 a random 1.66 s window, and four fixed spatial points over all three experiments in a random
738 1.66 s window. The null hypothesis states that medians of all three mean acceleration
739 distributions are equal, and the alternate hypothesis states that the mean accelerations
740 experienced by these groups are different. Significance level is $\alpha = 0.05$.

Source	**SS**	**df**	**MS**	χ^2	**P**
Unforced regime					
Group	5.54×10^4	2	2.77×10^4	12.40	**0.002**
Error	9.71×10^5	228	4.26×10^4		
Total	1.02×10^6	230			
Forced regime					
Group	9.76×10^3	2	4.88×10^3	4.38	0.11
Error	3.51×10^5	160	2.19×10^3		
Total	3.60×10^5	162			

741
742
743
744
745
746
747
748
749

Figure Legends

Figure 1: (A) Sample image from field of view in the turbulence tank: larvae are bright white spots and polystyrene passive particles are small dim white specks. (B) Close up of individual larva (white spot) overlaid with annulus of local flow velocity field (white arrows) estimated using PIV. (C-E) Sample time series of diving (black curve) versus non-diving larva (grey curve), where the vertical black dashed line denotes dive onset time: vertical displacement due to larval swimming (C), vertical swimming velocity $\boldsymbol{w_s}$ (D), and flow acceleration magnitude $|\boldsymbol{a}|$ experienced by each larva (E).

Figure 2: Diving larval vertical swimming velocity time series in the unforced regime, aligned by dive onset time. Larvae display strong uniformity in time spent accelerating downward, maximum downward velocity, and time spent decelerating out of the dive. Larvae exhibit a range of vertical swimming velocities prior to dive onset.

Figure 3: Values of hydromechanical parameters (mean and 95% confidence intervals) for diving larvae (black) and non-diving larvae (grey) in unforced and forced regimes. Values are calculated in a 1.66 s time interval prior to the dive onset in diving larvae, and a randomly selected 1.66 s time interval in the trajectories of non-diving larvae. Sample sizes are $n = 82$ for both groups in the unforced regime, and $n = 57$ in the forced regime. (A) Mean acceleration magnitude $|\boldsymbol{a}|$ is significantly different between diving and non diving larvae for both turbulence regimes (see Table 1). (B) Mean shear strain rate magnitude $|\boldsymbol{e_{xz}}|$ experienced by diving and non-diving larvae is not significantly different in either turbulence regime (Web Appendix Table

A2). (C-D) Mean horizontal and vertical normal strain rates $\boldsymbol{e_{xx}}$ and $\boldsymbol{e_{zz}}$ experienced by diving and non-diving larvae are not significantly different in either turbulence regime (Web Appendix Table A1). (E) Mean vorticity magnitude $|\boldsymbol{\omega_y}|$ experienced by diving and non-diving larvae is not significantly different in either turbulence regime (Web Appendix Table A2). (F) Mean angular acceleration magnitude $|\boldsymbol{\alpha}|$ experienced by diving and non-diving larvae is not significantly different in either turbulence regime (Web Appendix Table A2).

Figure 4: Probability distributions of mean flow acceleration magnitude experienced by larvae in a 1.66 s time interval (prior to dives for diving larvae, randomly selected for non-diving larvae), in unforced (A) and forced (B) regimes, respectively. The black bar distributions are those of diving larvae, $\boldsymbol{P}(|\boldsymbol{a}|_{\mathbf{1.66}}|\ \mathbf{larva\ dives})$, the grey bar distributions are those of non-diving larvae, $\boldsymbol{P}(|\boldsymbol{a}|_{\mathbf{1.66}}|\ \mathbf{larva\ does\ not\ dive})$, and the black dashed curves are background mean acceleration magnitudes $\boldsymbol{P}(|\boldsymbol{a}|_{\mathbf{1.66}})$. Note the different acceleration scales in unforced and forced regimes.

Figure 5: Probability of larval dive conditioned on $|\boldsymbol{a}|_{\mathbf{1.66}}$, the local mean acceleration field (averaged over 1.66s window), i.e. $\boldsymbol{P}(\mathbf{larva\ dives}|\ |\boldsymbol{a}|_{\mathbf{1.66}})$, for the unforced regime. Larvae were more likely to dive when they encountered higher local flow acceleration. Shaded grey region represents the 95% confidence interval for all mean accelerations.

794 **Figures**

795 Figure 1

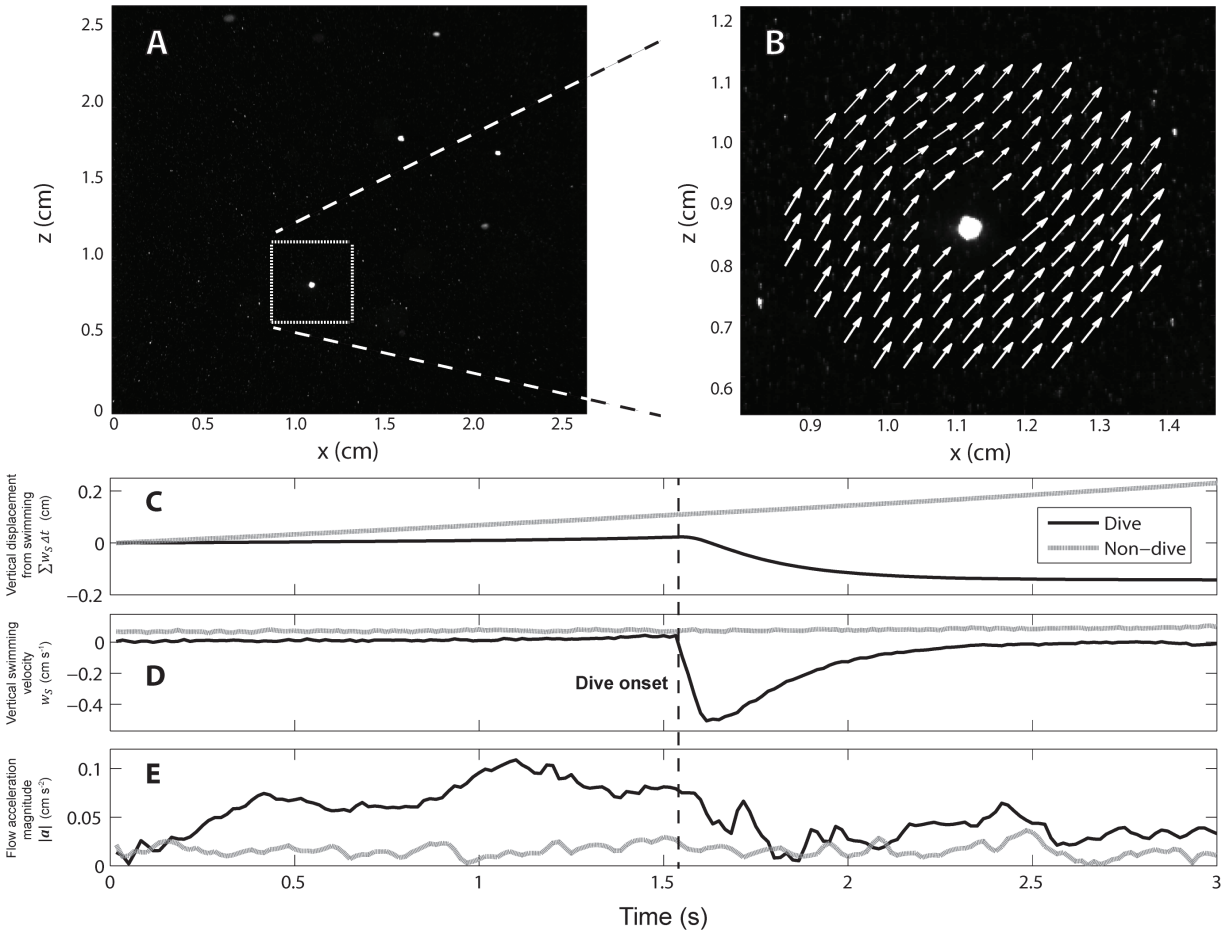

796

797

798

799

800

801 Figure 2

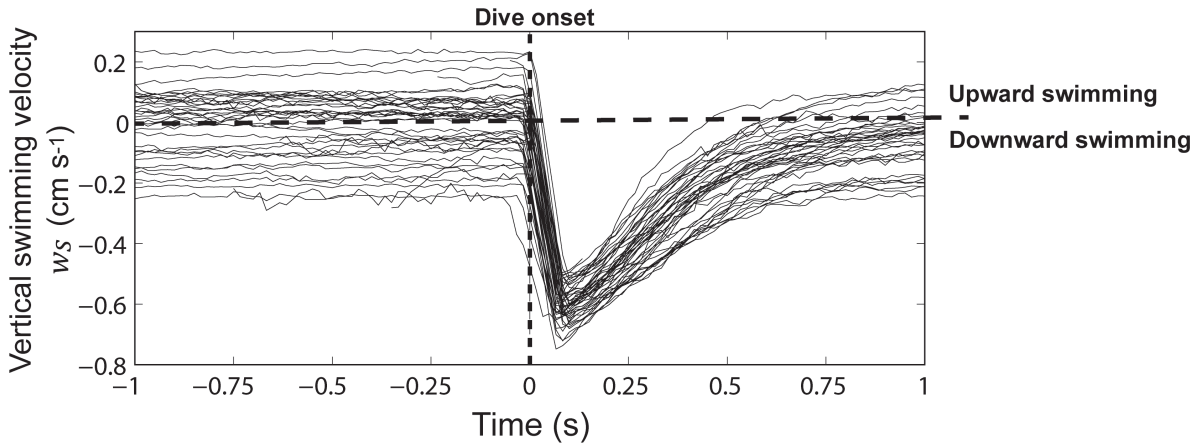

802

803

804

805

806

807

808

809

810

811

812

813

814 Figure 3

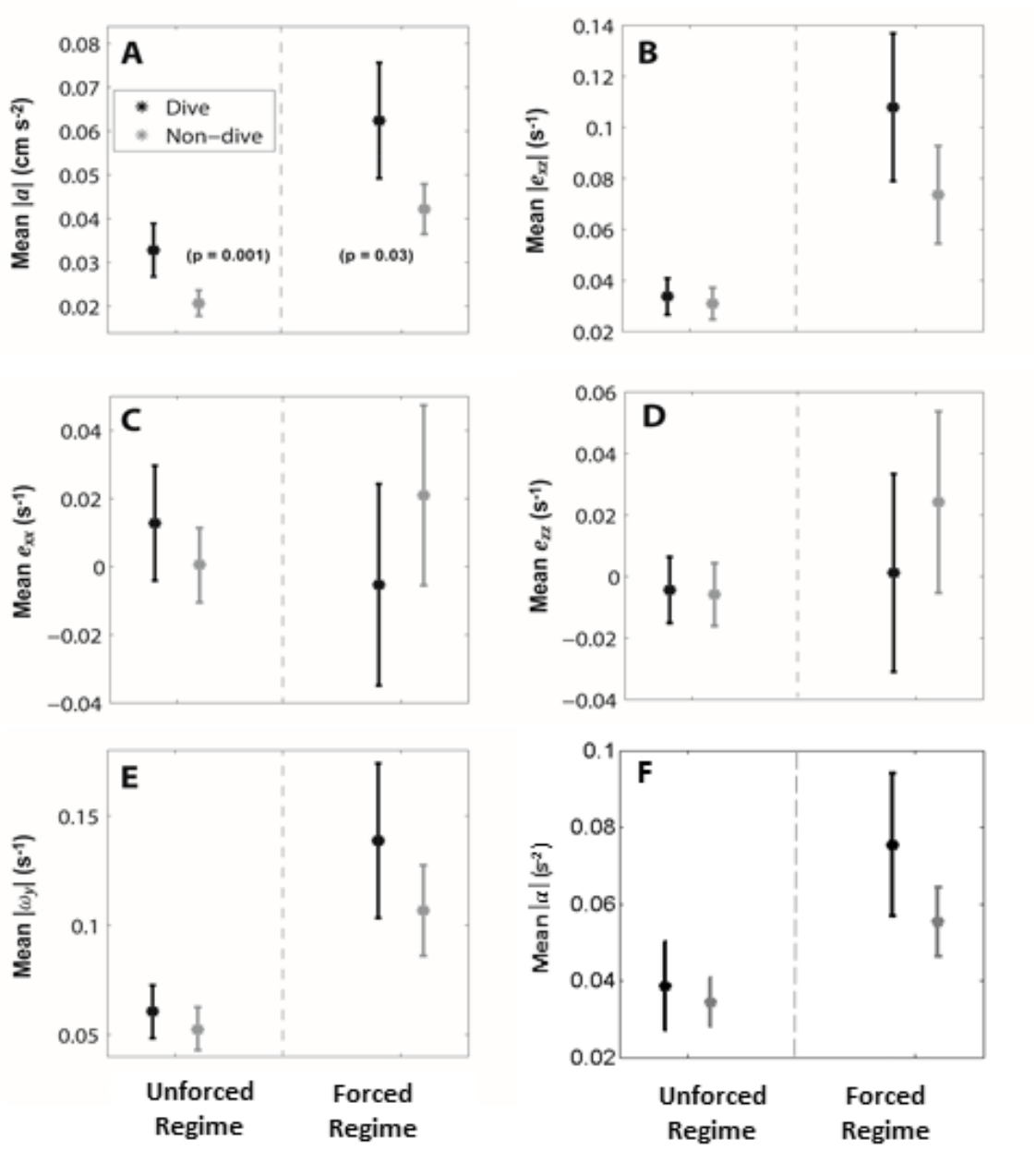

815

816

817

Figure 4

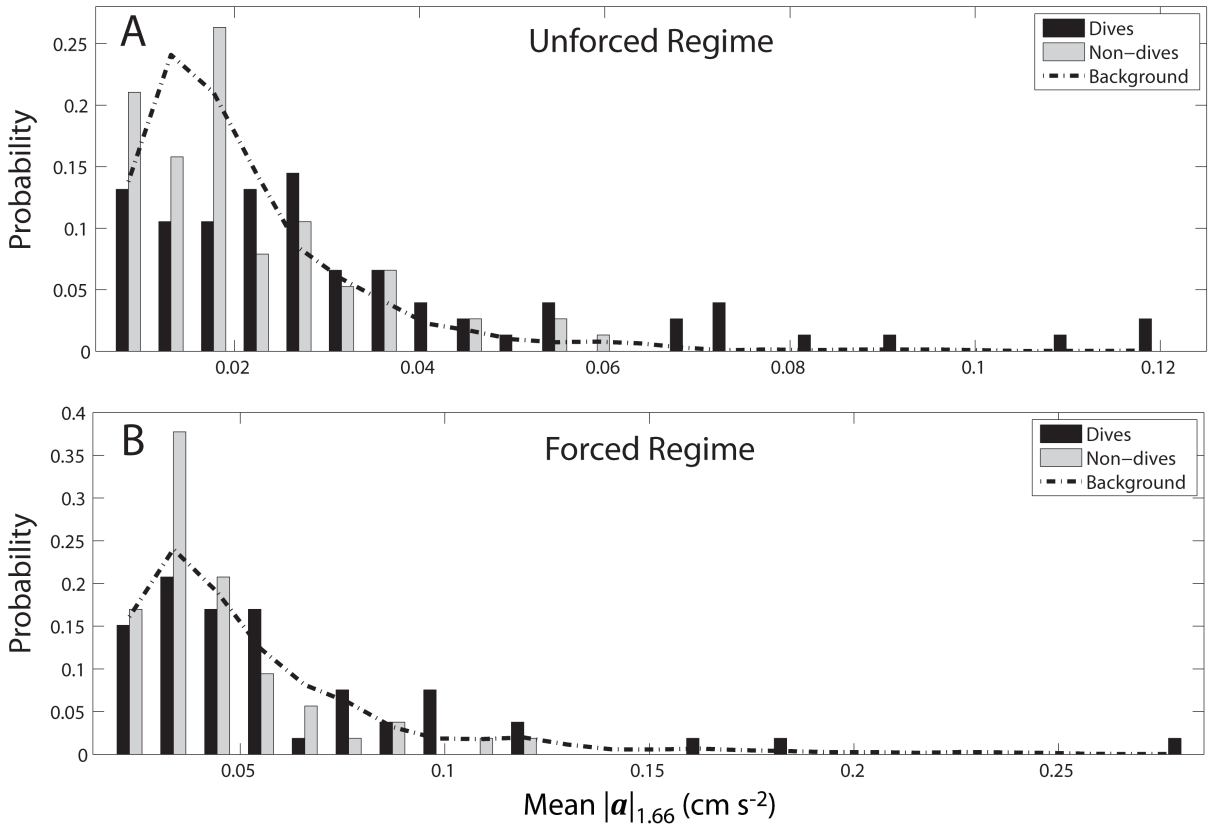
A
Unforced Regime
Dives
Non–dives
Background
Probability
0.25
0.2
0.15
0.1
0.05
0
0.02
0.04
0.06
0.08
0.1
0.12
B
Forced Regime
Dives
Non–dives
Background
Probability
0.4
0.35
0.3
0.25
0.2
0.15
0.1
0.05
0
0.05
0.1
0.15
0.2
0.25
Mean $|\boldsymbol{a}|_{1.66}$ (cm s^{-2})

830 Figure 5

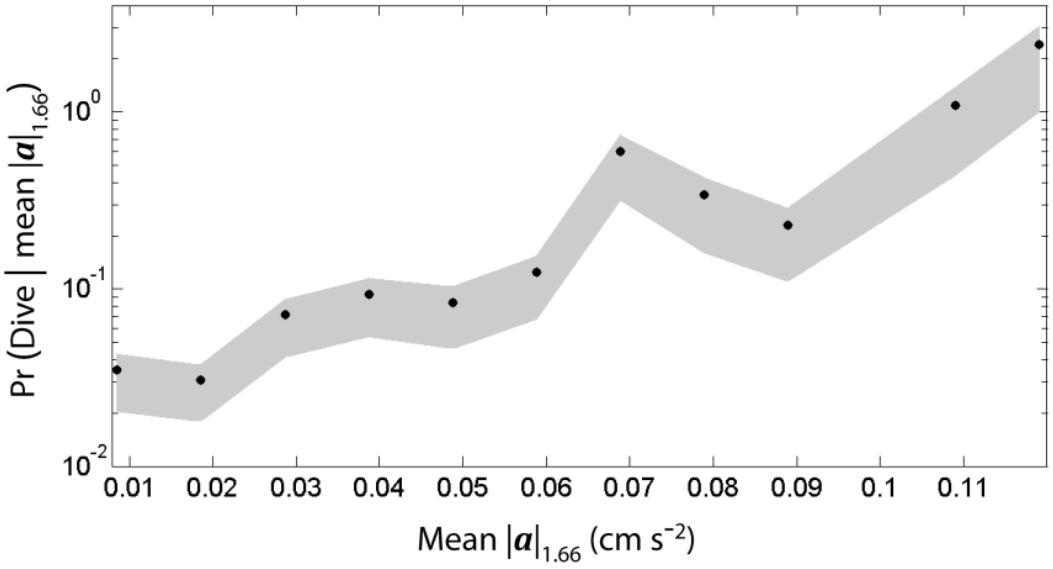

831

832

833